Int. J. Electrochem. Sci., 7 **(2012)** 1251 - 1265

International Journal of
ELECTROCHEMICAL
SCIENCE
www.electrochemsci.org

Synthesis and Catalytic Performance of PtRuMo Nanoparticles Supported on Graphene-Carbon Nanotubes Nanocomposites for Methanol Electro-Oxidation

Fei Ye[1], *Xiaorong Cao*[1], *Lin Yu*[1,*], *Shengzhou Chen*[2], *Weiming Lin*[2]

[1] Faculty of Chemical Engineering and Light Industry, Guangdong University of Technology, Guangzhou 510006, China
[2] School of Chemistry and Chemical Engineering, Guangzhou University, Guangzhou 510006, China
[*]E-mail: gych@gdut.edu.cn

Received: 17 November 2011 / *Accepted:* 29 December 2011 / *Published:* 1 February 2012

Graphene-carbon nanotubes (G-CNTs) nanocomposites supported PtRuMo catalyst was synthesized by chemical reduction of metal precursors with sodium borohydride at room temperature. The crystallographic properties, morphology and composition of the catalysts were characterized by X-ray diffraction (XRD), transmission electron microscopy (TEM) and energy dispersive X-ray (EDX), and the catalytic performance for methanol electro-oxidation was measured by CO stripping voltammetry, cyclic voltammetry (CV), linear sweep voltammetry (LSV), chronoamperometry (CA) and electrochemical impedance spectroscopy (EIS). The results show that the catalytic activity and stability of the PtRuMo/G-CNTs catalyst are higher than those of PtRuMo/G and PtRuMo/CNTs catalysts. The improved catalytic performance of PtRuMo/G-CNTs could be related to the higher electrochemically active surface area of PtRuMo nanoparticles due to the prevention of the restacking of graphene as well as the enhancement of the electronic conductivity and the mass transport of the reactants, products and electrolytes in G-CNTs nanocomposites.

Keywords: Graphene, carbon nanotubes, G-CNTs nanocomposites, PtRuMo/G-CNTs, methanol electro-oxidation

1. INTRODUCTION

Fuel cells, as a green power source to efficiently transform the chemical energy of fuels to electricity, have been receiving much attention in recent years due to the depletion of fossil fuels and

the increase in environmental pollution [1]. Among different types of fuel cells, direct methanol fuel cells (DMFCs) are the most promising power source for portable and small devices because of their advantages of high energy density, low pollutant emission, low operating temperature, and ease of handling liquid fuel [2]. However, there are some problems in the commercialization of DMFCs. For instance, the slow reaction kinetics of methanol electro-oxidation and methanol crossover must be overcome. Most commonly used Pt catalyst shows slow kinetics for methanol electro-oxidation, which is caused by self-poisoning of Pt catalyst surface [3]. Therefore, considerable efforts have been devoted to modify the Pt catalyst with other elements, such as Ru, W, Mo, Ni, Ce, Co, and so forth [4-8]. Many binary catalysts have been reported and PtRu is considered as the best binary catalyst because Ru takes part in a bifunctional mechanism with part of Ru atoms in oxidized state supplying oxygenated species necessary for complete oxidation of methanol to CO_2 and other part of Ru atoms alloyed with Pt to weaken Pt-CO bond [9]. However, because of the insufficient efficiency and high cost of PtRu, further optimization of the catalyst is crucial for its practical application.

The most common solution is to employ ternary catalysts with other cheap metals or metal oxides, and disperse the catalytic nanoparticles on appropriate supports. Earlier investigations have demonstrated that PtRuMo catalyst exhibits remarkable activity for methanol electro-oxidation [10-18], which may be attributed to the electronic effect, the bifunctional mechanism, and the hydrogen spillover effect [19]. PtRuMo nanoparticles are generally supported on carbon black (Vulcan XC-72), carbon nanotubes [19-21], and occasionally supported on polyaniline [22], graphite felt [23] and carbon nanofibers [24]. However, to the best of our knowledge, no work has been done on the PtRuMo nanoparticles supported on other carbon nanomaterials or nanocomposites.

The catalyst support plays an important role in the performance of the catalysts. The supports for fuel cell catalysts must possess appropriate structure and specific surface area, electronic conductivity, anti-corrosion, and so forth [25]. Generally, Vulcan XC-72 carbon black is the common support for fuel cell catalysts. However, the catalyst utilization is low in Vulcan XC-72 supported catalysts, because most of the pores in Vulcan XC-72 are in the micro region, which leads to poor electrochemically active surface area (EASA) as the catalytic nanoparticles within the micropores are inaccessible to the fuels. Thus, new carbon materials have been developed to improve the catalyst utilization and catalytic performance. For example, mesoporous carbons, carbon nanotubes (CNTs), nanofibers (CNFs), nanohorns (CNHs), nanocoils (CNCs) and graphene (G) have been studied extensively, due to their unique structure and electric properties [26]. CNTs with one-dimensional (1D) structure exhibit superior electronic conductivity and high electrochemical stability. Therefore, CNTs have been exploited as the catalyst support to enhance catalytic activity in fuel cells [27]. On the other hand, graphene, a two-dimensional (2D) carbon material with single (or a few) atomic layer, has unique physical properties such as high specific surface area (theoretical value of 2620 m^2 g^{-1}), superior electronic conductivity and excellent mechanical strength and elasticity [28]. Thus, graphene supported Pt and PtRu catalysts have been developed to improve the electro-catalytic performance for methanol oxidation and oxygen reduction [29-36]. However, there are some problems for the use of

graphene as catalyst support. For instance, because of the van der Waals interaction, the reduced graphene nanosheets tend to form irreversible agglomerates and even restack to form graphite during the reduction of graphene oxide (GO) [37]. The attachment of three-dimensional (3D) metal/alloy nanoparitles (e. g., Pt, PtRu, PtRuMo) onto the graphene may, to some extent, prevent the restacking of graphene nanosheets during the chemical reduction process. Meanwhile, the restacking can also be prevented by using CNTs as nanospacers to increase the EASA and catalytic performance [38]. It is anticipated that metal nanoparticles dispersed in graphene-carbon nanotubes(G-CNTs) nanocomposites, a unique combination of 3D, 2D and 1D structure, would improve the catalytic performance of methanol electro-oxidation. Lv et al. [39] synthesized nitrogen-doped carbon nanotube-graphene hybrid nanostructure (NCNT-GHN) by a one-step water-assisted chemical vapor deposition (CVD) route and used it to support well-dispersed PtRu nanoparticles for application as high-performance methanol electro-oxidation catalyst. Compared to commercial and CNTs supported PtRu catalysts, a much better catalytic performance was achieved by a synergistic effect of the hierarchical structure (G-CNT hybrid) and electronic modulation (N-doping) during the methanol electro-oxidation. Jafri et al. [40,41] reported that Pt and PtRu nanoparticles supported on functionalized graphene-functionalized multiwalled carbon nanotube hybrid (Pt/f-G-f-MWNT and PtRu/f-G-f-MWNT) show higher electro-catalytic activities for oxygen reduction and methanol oxidation with respect to those supported on f-G or f-MWNT. However, the preparation of f-G required high temperature (thermal exfoliation of GO at 1050 °C) and strong acid treatment (concentrated HNO_3 and H_2SO_4), which are not favorable for practical application. Since GO and metal precursors can be simultaneously reduced by reducing agents such as $NaBH_4$, ethylene glycol, 1,2-propanediol, and so forth [29,42], it's desirable to use GO instead of f-G as the starting material for graphene.

We have reported that CNTs supported PtRuMo catalyst showed higher catalytic activity towards methanol electro-oxidation when compared with CNTs supported PtRu catalyst and commercial PtRu/C catalyst [19]. In this study, we synthesized PtRuMo nanoparticles supported on graphene-carbon nanotubes nanocomposites (PtRuMo/G-CNTs) by using a mixture solution of GO and CNTs as the starting materials, and evaluated its catalytic performance for methanol electro-oxidation with various electrochemical measurements. In comparison with PtRuMo/CNTs and PtRuMo/G catalysts, PtRuMo/G-CNTs catalyst exhibits higher catalytic performance because of its larger electrochemically active surface area.

2. EXPERIMENTAL

2.1 Preparation of catalysts

For the synthesis of graphene, GO was first prepared by an improved Hummers method [43,44]. PtRuMo (with an atomic ratio of 6:3:1) catalysts supported on three different supports were

prepared by chemical reduction of H_2PtCl_6, $RuCl_3$ and Na_2MoO_4 precursors with sodium borohydride at room temperature. The metal loading of the catalyst was 30% in weight. Briefly, for the synthesis of PtRuMo/G-CNTs catalyst, appropriate amount of support (GO and CNTs with weigh ratio of 1:1), metal precursors, and ethylene glycol were ultrasonically mixed for 30 min and then mechanically stirred for 3 h. Excess quantities of 0.2 $mol \cdot L^{-1}$ sodium borohydride in ethylene glycol were added drop-by-drop to the mixed solution, and then the bath was stirred for 12 h for the complete reduction of the GO and metal precursors. Finally, the mixtures were filtered, washed, and dried by freeze-drying method. For comparison purpose, PtRuMo/G and PtRuMo/CNTs catalysts were also prepared by the same method.

2.2 Characterizations of catalysts

X-ray diffraction (XRD) powder patterns of the catalysts were obtained on a XD-3 X-ray diffractometer (Beijing Purkinje General Instrument Co., Ltd., China) using a Cu-K_α source operating at 36 kV and 20 mA. The scanning range and rate are 5°-90° and 2° min^{-1}, respectively. The TEM micrographs were recorded with a Philips Tecnai-10 operating at 100 kV. Chemical composition analysis of the catalysts was carried out on an energy dispersive X-ray (EDX) analyzer (Oxford INCA300) attached to a scanning electron microscope (LEO 1530 VP, Germany).

2.3 Electrochemical measurements

The electrochemical measurements were performed in a solution of 0.5 $mol \cdot L^{-1}$ H_2SO_4 and 1.0 $mol \cdot L^{-1}$ CH_3OH at room temperature, using a conventional three electrode cell and a Solartron SI 1287 electrochemical interface and SI 1260 impedance/gain-phase analyzer. A Pt mesh and a saturated calomel electrode (SCE, -0.241 V vs. NHE) were used as counter electrode and reference electrode, respectively. The catalyst modified glassy carbon (GC) electrode was used as the working electrode. The GC electrode was polished by 1.0, 0.3 and 0.05 μm alumina (CHI Inc., USA), respectively, and then washed in ethanol and ultra-pure water ultrasonically. 2 mg catalyst and 1 ml solution (20.00% isopropanol+73.75% H_2O+6.25% Nafion (5 wt%, Fluka)) were mixed ultrasonically for 30 min. Then 6 μl slurry was pipetted onto the surface of the polished GC electrode. After the solvent evaporation, the working electrode was obtained. The apparent surface area of the GC electrode was 0.07 cm^2, and the specific loading of the catalyst was about 51.43 μg_{metal} cm^{-2}.

For the CO stripping voltammetry, carbon monoxide (99.9% pure) was absorbed onto the catalyst by bubbling it in the supporting electrolyte of 0.5 $mol \cdot L^{-1}$ H_2SO_4 solution for 20 min, while the potential was held at -0.091 V vs. SCE. Then a pure N_2 stream was purged for 30 min to remove the CO dissolved in the H_2SO_4 solution, and the potential was then cycled from -0.091 V to 0.759 V vs. SCE for one cycle and -0.241 V to 0.759 V vs. SCE for two cycles with a scanning rate of 10 mV/s. Cyclic Voltammograms (CV) were plotted in a solution of 0.5 $mol \cdot L^{-1}$ H_2SO_4+1.0 $mol \cdot L^{-1}$ CH_3OH

within a potential range between -0.241 and 0.759 V vs. SCE with a scanning rate of 20 mV/s. Linear sweep voltammetry (LSV) were plotted within a potential range from -0.241 to 0.459 V vs. SCE with a scanning rate of 5 mV/s, and the chronoamperometry (CA) profiles were obtained at a potential of 0.30 V vs. SCE with a polarization time of 15 min. The impedance spectra were registered at frequencies from 100 KHz to 0.01 Hz with an amplitude of 10 mV at a potential of 0.40 V vs. SCE, and ZPlot and ZView softwares were used to measure and analyze the impedance data, respectively.

3. RESUTLTS AND DISCUSSION

3.1 Characterization of the catalysts

The X-ray diffraction patterns of GO and the synthesized catalysts are presented in Fig. 1. The diffraction peak of GO at 10.9°, which is corresponding to (001) plane of GO [45], is observed with a interlayer space (d-spacing) of 0.802 nm. This is larger than the d-spacing (0.34 nm) of graphite (2θ=26.5°) because of the oxygenated functional groups on the carbon nanosheets introduced during the oxidation of graphite. For PtRuMo/G and PtRuMo/G-CNTs catalysts, after the GO and metal precursors were reduced by $NaBH_4$, the characteristic peak of GO located at 10.9° disappears completely and a broad peak appears at around 22.8°, confirming the complete reduction of GO and the formation of layered graphene nanosheets [46]. The peak located at about 25.5° in the PtRuMo/CNTs and PtRuMo/G-CNTs catalysts is associated with the (002) plane of carbon support. For all the three samples, four characteristic peaks corresponding to (111), (200), (220), and (311) planes of the fcc crystalline Pt are observed, and the corresponding peak angles are a little shift to higher 2θ values of 39.76°, 46.24°, 67.45° and 81.28° for pure Pt fcc, indicating that the alloy catalysts have single phase disordered structures, and the lattice constants decrease because of Ru or Mo substitution in Pt fcc center. Neither peaks of Ru and Mo nor peaks of metal oxides are found. The peaks corresponding to PtRuMo nanoparticles supported on G-CNTs are broadened with respect to those supported on CNTs or graphene, indicating that PtRuMo nanoparticles with smaller particle size are highly dispersed on G-CNTs nanocomposites. In order to assess the particle size of the metallic clusters on the support, the (220) reflection of Pt fcc structure was further analyzed in detail. The average particle size may be roughly calculated from Pt (220) FWHM according to the Debye-scherrer equation (1) [47]:

$$L=0.9\lambda_{CuK\alpha}/(B_{2\theta}\cos\theta_{max}) \quad (1)$$

where L is the average particle size, $\lambda_{CuK\alpha}$ is the X-ray wave-length (1.5406 Å), $B_{2\theta}$ is the full width at half maximum, and θ_{max} is the angle at peak maximum. The results are presented in Table 1. The average particle sizes for PtRuMo/CNTs, PtRuMo/G and PtRuMo/G-CNTs catalysts are 3.3, 3.0

and 2.2 nm, respectively. It's clear that the introduction of CNTs between graphene nanosheets reduces the average particle size of PtRuMo nanoparticles.

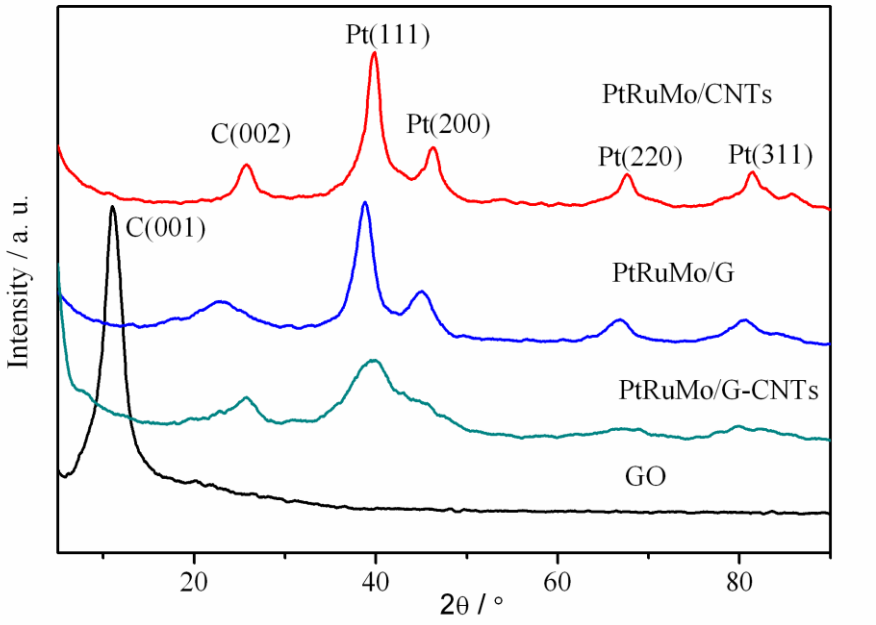

Figure 1. XRD patterns of GO and the catalysts

Table 1. Average particle sizes, atomic ratios and EASAs of the catalysts

Catalyst	Average crystal size (nm)	Pt:Ru:Mo atomic ratio	EASA ($m^2 g^{-1}$)
PtRuMo/CNTs	3.3	55:28:17	32.08
PtRuMo/G	3.0	56:29:15	60.62
PtRuMo/G-CNTs	2.2	60:28:12	125.43

Fig. 2a and Fig. 2b show the TEM images of PtRuMo/G and PtRuMo/G-CNTs catalysts, respectively. It can be seen from Fig. 2a that PtRuMo nanoparticles are homogenously dispersed on the graphene nanosheets with some agglomeration. Similarly, Fig. 2b shows the homogenous dispersion of PtRuMo nanoparticles on the surfaces of CNTs and graphene. EDX spectra of PtRuMo/CNTs, PtRuMo/G and PtRuMo/G-CNTs catalysts, as shown in Fig. 3, confirm the presence of PtRuMo nanoparticles on the supports, and the metal atomic ratios are listed in Table 1. The atomic ratios of PtRuMo/CNTs, PtRuMo/G and PtRuMo/G-CNTs catalysts are 55:28:17, 56:29:15 and 60:28:12, respectively, which are close to the theoretical values.

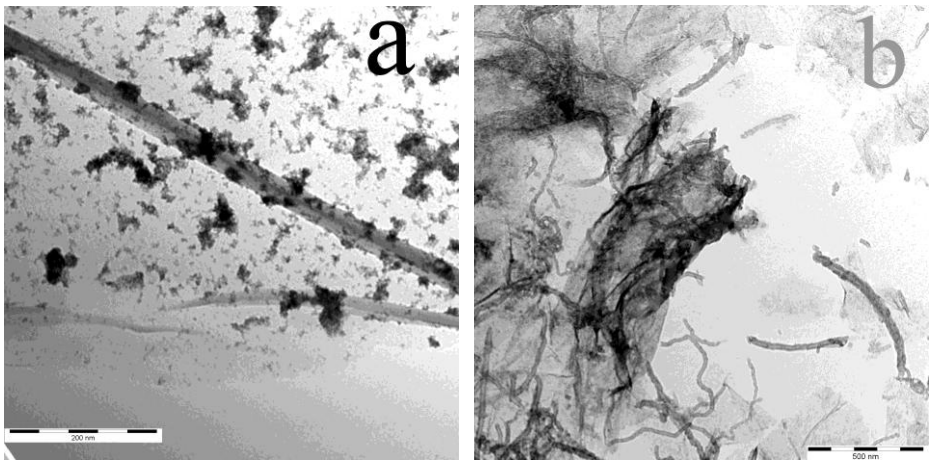

Figure 2. TEM images of PtRuMo/G (a) and PtRuMo/G-CNTs (b)

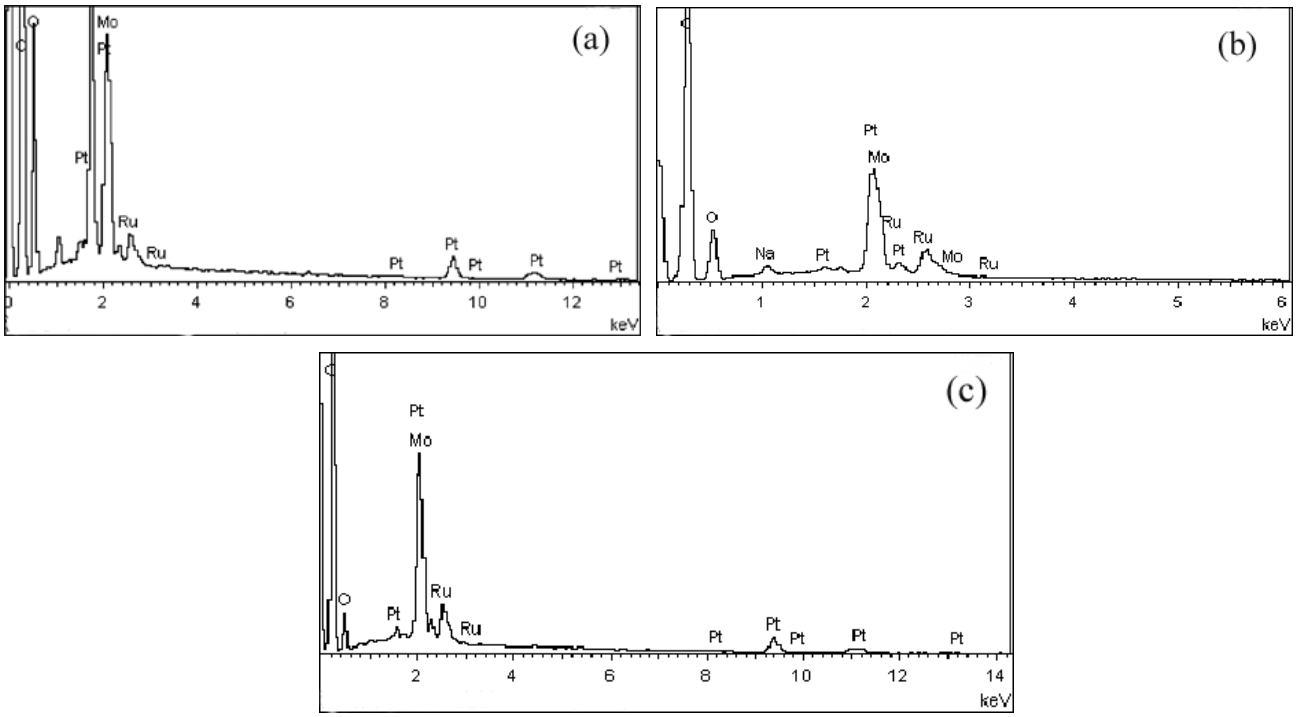

Figure 3. EDX spectra of PtRuMo/CNTs (a), PtRuMo/G (b) and PtRuMo/G-CNTs (c)

3.2 Electrochemical measurements of the catalysts

CO stripping experiments were used to estimate the EASA of the catalysts, which is an important index about the number of available active sites of the catalysts. Fig. 4 shows the cyclic voltammograms during the 3 cycles after the catalysts were pre-absorbed with CO at -0.091 V vs. SCE for 20 min. In the first cycle, an anodic peak corresponding to the oxidation of absorbed CO is

observed. In the following 2 cycles, the peak related to CO oxidation is no longer present, indicating that the entire pre-absorbed CO was completely oxidized during the first cycle. The EASA of the catalyst may be roughly calculated by the following equation (2) [48,49]:

$$S_{EASA}=Q_{co}/[m_{metal}\times 420(\mu C\ cm^{-2})] \quad (2)$$

where Q_{CO} is the charge for CO desorption electro-oxidation in microcoulomb (μC) and m_{metal} is the metal loading of the catalyst in the electrode, assuming an adsorption charge of 420 μC cm^{-2} for a CO monolayer. The results are showed in Table 1. It is interesting to note that PtRuMo/G-CNTs (125.43 m^2 g^{-1}) catalyst exhibits larger electrochemically active surface area when compared with PtRuMo/CNTs (32.08 m^2 g^{-1}) and PtRuMo/G (60.62 m^2 g^{-1}) catalysts.

The highest EASA of PtRuMo/G-CNTs catalyst is indicative of best accessibility of catalyst active sites, which could be attributed to the unique hierarchical graphene-CNTs architecture as well as the smaller particle size of PtRuMo nanoparticles (Table 1).

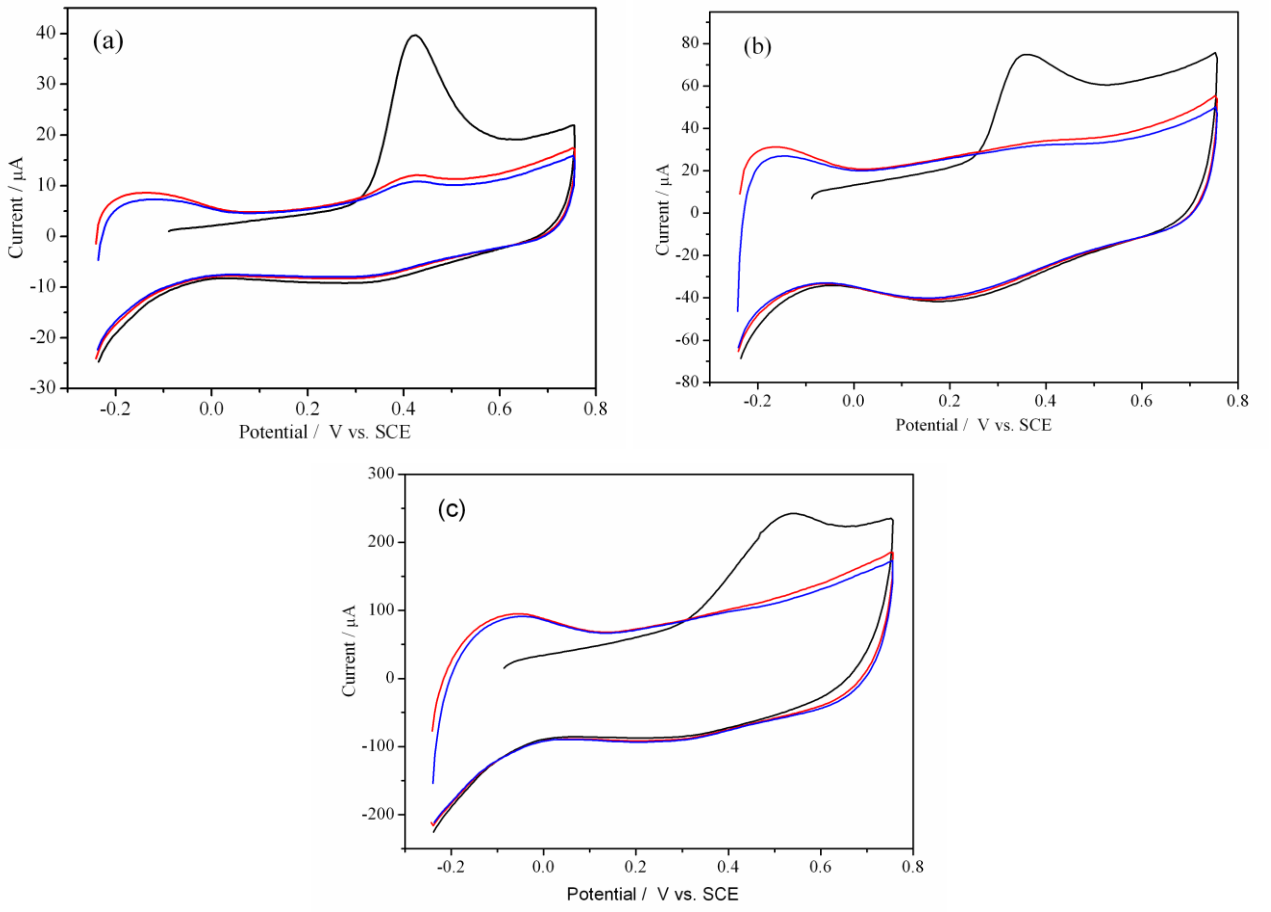

Figure 4. CO-stripping voltammograms of PtRuMo/CNTs (a), PtRuMo/G (b) and PtRuMo/G-CNTs (c) in 0.5 mol·L^{-1} H_2SO_4 solution at room temperature, with a scan rate of 10 mV/s

Fig. 5 shows cyclic voltammograms of methanol electro-oxidation over the catalysts. Two methanol oxidation peaks, corresponding to electro-oxidation of methanol in forward scan and its intermediates in reverse scan, are observed.

Value of peak current density is directly proportional to catalytic activity of the catalyst. The values of peak current densities for different catalysts are listed in Table 2. It is apparent from Table 2 that the peak current density for PtRuMo/G-CNTs catalyst is higher than those of PtRuMo/CNTs and PtRuMo/G catalysts, suggesting that the mixed support of G-CNTs nanocomposites can improve the activity of PtRuMo catalyst for methanol electro-oxidation. The larger electrochemically active surface area and smaller particle size of PtRuMo/G-CNTs catalyst could contribute to its better activity towards methanol electro-oxidation.

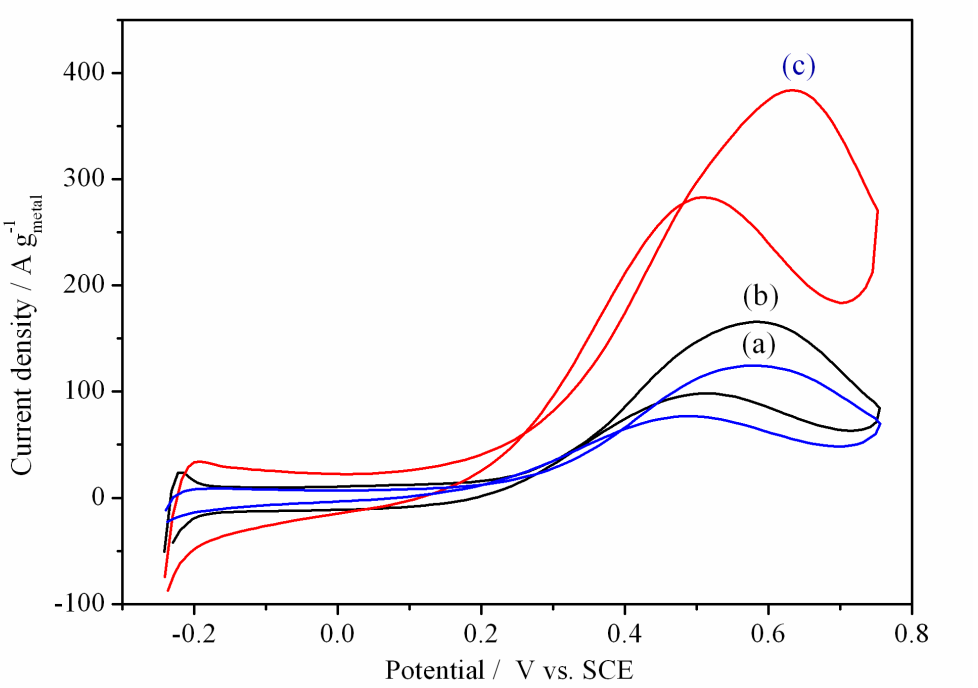

Figure 5. Cyclic voltammograms for methanol electro-oxidation on PtRuMo/CNTs (a), PtRuMo/G (b) and PtRuMo/G-CNTs (c) in 0.5 mol·L^{-1} H_2SO_4 + 1.0 mol·L^{-1} CH_3OH solution at room temperature, with a scan rate of 20 mV/s

Table 2. Electrochemical properties of the catalysts

Catalysts	Peak current density (A g^{-1})	Current density at 900 s (A g^{-1})	R_{ct} (Ω)
PtRuMo/CNTs	124	5.5	829
PtRuMo/G	166	36.1	548
PtRuMo/G-CNTs	384	38.4	250

The catalytic activities of the catalysts were also analyzed by linear sweep voltammetry with scanning from -0.241 to 0.459 V vs. SCE at a scan rate of 5 mV/s, and the results are showed in Fig. 6. Theoretically, methanol electro-oxidation may proceed at 0.04 V vs. NHE, but the potential for methanol electro-oxidation on Pt-based catalysts is much higher than the theoretical value due to the poisoning of Pt active sites by the reaction intermediates, such as formaldehyde, formic acid, carbon monoxide, and so forth [50]. According to Fig. 6, the onset potential of methanol electro-oxidation on the PtRuMo/G-CNTs catalyst is similar to those of PtRuMo/CNTs and PtRuMo/G catalysts. However, the PtRuMo/G-CNTs catalyst shows a higher current density at the whole potential rang than those of PtRuMo/CNTs and PtRuMo/G catalysts, indicating superior catalytic activity.

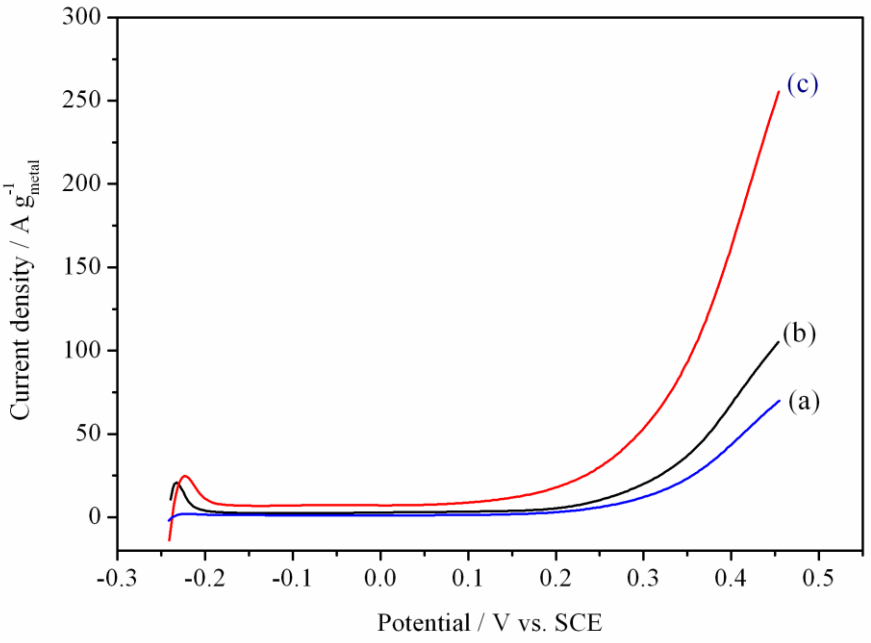

Figure 6. Linear sweep voltammetries of methanol electro-oxidation on PtRuMo/CNTs (a), PtRuMo/G (b) and PtRuMo/G-CNTs (c) in 0.5 mol·L^{-1} H_2SO_4 and 1.0 mol·L^{-1} CH_3OH solution at room temperature, with a scan rate of 5 mV/s

To further confirm the catalytic activities and stabilities of PtRuMo catalysts for methanol electro-oxidation, chronoamperometric experiments were carried out at a given potential. The chronoamperometry profiles of methanol electro-oxidation on the PtRuMo/CNTs, PtRuMo/CNTs and PtRuMo/G-CNTs catalysts at a potential of 0.30 V vs. SCE are shown in Fig. 7. It can be seen from Fig. 7 that for all the three catalysts, the recorded currents decrease gradually with the test time, which may be due to the poisoning of Pt active sites by the intermediate species of methanol electro-oxidation. PtRuMo/G-CNTs catalyst has the highest current density throughout the test time, and the current density at 900 s at PtRuMo/G-CNTs (38.4 A g^{-1}) electrode is larger than those at PtRuMo/G

(36.1 A g^{-1}) and PtRuMo/CNTs (5.5 A g^{-1}) electrodes (Table 2). These results further demonstrate the improved catalytic activity and stability of PtRuMo/G-CNTs catalyst in comparison to PtRuMo/G and PtRuMo/CNTs catalysts.

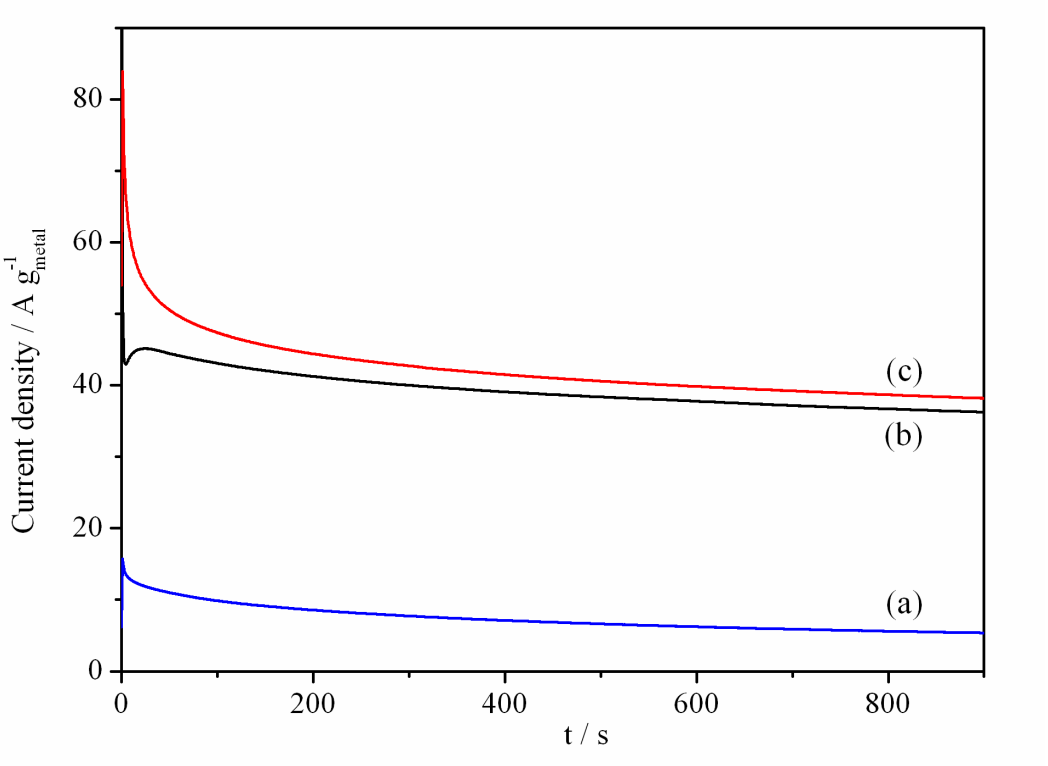

Figure 7. Chronoamperometry profiles of methanol electro-oxidation on PtRuMo/CNTs (a), PtRuMo/G (b) and PtRuMo/G-CNTs (c) in 0.5 mol·L^{-1} H_2SO_4 + 1.0 mol·L^{-1} CH_3OH solution at a potential of 0.30 V vs. SCE at room temperature

Electrochemical impedance spectroscopy was used to determine the charge transfer resistance (R_{ct}) during the methanol oxidation process on the catalysts. Fig. 8 shows the Nyquist plots of the catalysts obtained in a solution of 0.5 mol·L^{-1} H_2SO_4 and 1.0 mol·L^{-1} CH_3OH solution at a potential of 0.40 V vs. SCE. In the Nyquist plot, a semicircle which cuts the real axis is observed, and an inductive loop appears at low frequencies.

Similar results have been reported for Pt, PtRu and PtRuNi catalysts, with the inductive behavior attributed to the kinetic of CO oxidation [51-54]. The impedance data were fitted by using the ZView software and equivalent circuit [55], and the values of various circuit elements were obtained. The R_{ct} values are 829 Ω, 548 Ω and 250 Ω for PtRuMo/CNTs, PtRuMo/G and PtRuMo/G-CNTs catalysts, respectively. A significant decrease of the R_{ct} value for PtRuMo/G-CNTs catalyst indicates a smaller reaction resistance of methanol electro-oxidation and higher catalytic activity for PtRuMo/G-CNTs catalyst.

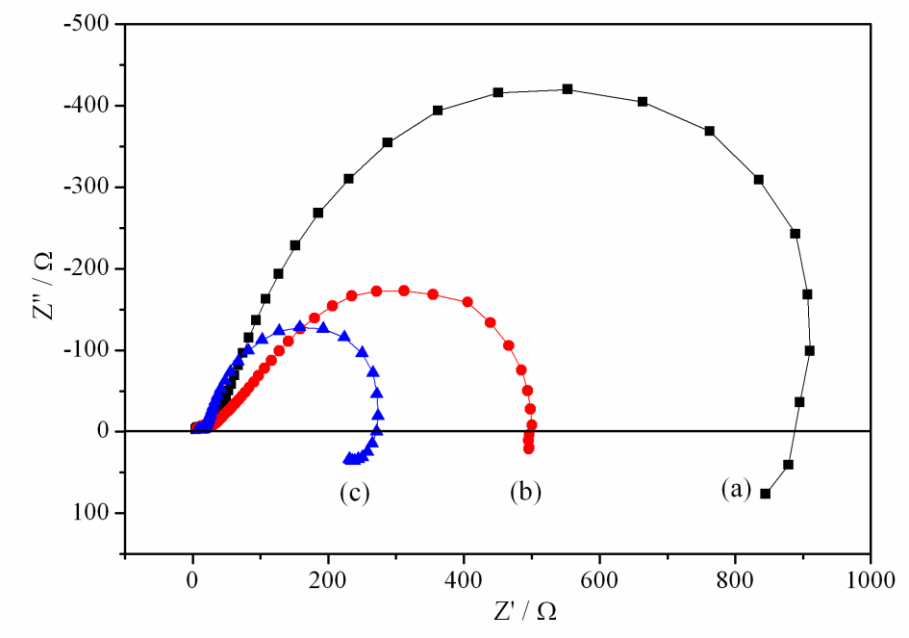

Figure 8. Nyquist plots for PtRuMo/CNTs (a), PtRuMo/G (b) and PtRuMo/G-CNTs (c) in 0.5 mol·L^{-1} H_2SO_4 + 1.0 mol·L^{-1} CH_3OH solution at a potential of 0.40 V vs. SCE at room temperature

It is observed from the electrochemical measurements that the introduction of CNTs between the graphene nanosheets can further improve the catalytic performance of PtRuMo catalyst for methanol electro-oxidation. The improved catalytic performance could be ascribed to the synergistic effect between CNTs and graphene nanosheets on decreasing the particle sizes of PtRuMo nanoparticles and increasing the EASA of PtRuMo/G-CNTs catalyst. This synergistic effect can be explained in three aspects. Firstly, CNTs as a nanospacer can reduce the π-π interaction between graphene nanosheets resulting from steric hindrance to prevent the restacking of graphene [38,56]. Secondly, CNTs can bridge the gaps between graphene nanosheets to form a 3D conductive network, providing efficiently conductive pathways for electron conduction in the G-CNTs nanocomposites [57]. Thirdly, the 3D hierarchical G-CNTs architecture provides highly porous and open channels leading to the better mass transport of reactants, products and electrolytes [38,58]. Thus, CNTs may act as a nanospacer, electronic conductivity promoter and pore former in the G-CNTs nanocomposites to enhance the catalytic performance of PtRuMo/G-CNTs catalyst for methanol electro-oxidation.

4. CONCLUSIONS

Graphene-carbon nanotubes nanocomposites supported PtRuMo catalyst was synthesized by borohydride reduction method and applied for methanol electro-oxidation. XRD, TEM and EDX indicate that PtRuMo nanoparticles are homogenously dispersed on the surfaces of graphene and

CNTs. The activity and stability of PtRuMo/G-CNTs catalyst for methanol electro-oxidation are higher than those of PtRuMo/G and PtRuMo/CNTs catalysts. The improved catalytic performance of PtRuMo/G-CNTs catalyst could be attributed to the good accessibility of PtRuMo nanoparticles for methanol electro-oxidation. CNTs may act as a nanospacer, electronic conductivity promoter and pore former in the G-CNTs nanocomposites to increase the exposing surface area of graphene, the electronic conductivity and the mass transport of reactants, products and electrolytes, and hence the PtRuMo/G-CNTs catalyst can provide more electrochemically active surface area for methanol electro-oxidation.

ACKNOWLEDGEMENTS
The authors thank the financial support by National Natural Science Foundation of China (21076048), Natural Science Foundation of Guangdong Province (S2011040005569, 10251009001000003), Guangdong Science and Technology Plan Project (2010B010900039) and Guangzhou Science and Technology Plan Project (2009J1-C431-1).

References

1. J.M. Andujar and F. Segura, *Renew. Sustain. Energy Rev.*, 13 (2009) 2309
2. S.K. Kamarudin, F. Achmad and W.R.W. Daud, *Int. J. Hydrogen Energy*, 34 (2009) 6902
3. X. Zhao, M. Yin, L. Ma, L. Liang, C. Liu, J. Liao, T. Lu and W. Xing, *Energ. Environ. Sci.*, 4 (2011) 2736
4. T.M. Marques, P.N.S.d. Oliveira, B. Michele, C.O. Vercino, V.J. Carlo, A.F. Jaco, N.A. Oliveira and S.E. Vitorio, *Int. J. Electrochem. Sci.*, 6 (2011) 484
5. S. Jayaraman, T.F. Jaramillo, S.H. Baeck and E.W. McFarland, *J. Phys. Chem. B*, 109 (2005) 22958
6. X. Zhou, R. Zhang, Z. Zhou and S. Sun, *J. Power Sources*, 196 (2011) 5844
7. Y.Y. Chu, Z.B. Wang, Z.Z. Jiang, D.M. Gu and G.P. Yin, *Adv. Mater.*, 23 (2011) 3100
8. R. Awasthi and R.N. Singh, *Int. J. Electrochem. Sci.*, 6 (2011) 4775
9. O.A. Petrii, *J. Solid State Electrochem.*, 12 (2008) 609
10. S. Pasupathi and V. Tricoli, *J. Solid State Electrochem.*, 12 (2008) 1093
11. K. Lasch, L. Jörissen and J. Garche, *J. Power Sources*, 84 (1999) 225
12. X. Zhang, F. Zhang and K.Y. Chan, *J. Mater. Sci.*, 39 (2004) 5845
13. M.V. Martinez-Huerta, J.L. Rodriguez, N. Tsiouvaras, M.A. Pena, J.L.G. Fierro and E. Pastor, *Chem. Mater.*, 20 (2008) 4249
14. K.R. Lee, M.K. Jeon and S.I. Woo, *Appl. Catal. B Environ.*, 91 (2009) 428
15. Z.B. Wang, P.J. Zuo and G.P. Yin, *Fuel Cells*, 9 (2009) 106
16. M.V. Martínez-Huerta, N. Tsiouvaras, M.A. Peña, J.L.G. Fierro, J.L. Rodríguez and E. Pastor, *Electrochim. Acta*, 55 (2010) 7634
17. N. Tsiouvaras, M.V. Martínez-Huerta, O. Paschos, U. Stimming, J.L.G. Fierro and M.A. Peña, *Int. J. Hydrogen Energy*, 35 (2010) 11478
18. N. Tsiouvaras, M.A. Pena, J.L.G. Fierro, E. Pastor and M.V. Martinez-Huerta, *Catal. Today*, 158 (2010) 12
19. S. Chen, F. Ye and W. Lin, *Int. J. Hydrogen Energy*, 35 (2010) 8225

20. T. Huang, D. Zhang, L. Xue, W. Cai and A. Yu, *J. Power Sources*, 192 (2009) 285
21. N. Kakati, J. Maiti, J.Y. Oh and Y.S. Yoon, *Appl. Surf. Sci.*, 257 (2011) 8433
22. A. Lima, C. Coutanceau, J.M. Leger and C. Lamy, *J. Appl. Electrochem.*, 31 (2001) 379
23. A. Bauer, E.L. Gyenge and C.W. Oloman, *J. Power Sources*, 167 (2007) 281
24. N. Tsiouvaras, M.V. Martinez-Huerta, R. Moliner, M.J. Lazaro, J.L. Rodriguez, E. Pastor, M.A. Pena and J.L.G. Fierro, *J. Power Sources*, 186 (2009) 299
25. E. Antolini, *Appl. Catal. B Environ.*, 88 (2009) 1
26. S. Tang, G. Sun, J. Qi, S. Sun, J. Guo, Q. Xin and G.M. Haarberg, *Chin. J. Catal.*, 31 (2010) 12
27. N. Jha, A. Leela Mohana Reddy, M.M. Shaijumon, N. Rajalakshmi and S. Ramaprabhu, *Int. J. Hydrogen Energy*, 33 (2008) 427
28. D. Chen, L.H. Tang and J.H. Li, *Chem. Soc. Rev.*, 39 (2010) 3157
29. J. Li, Y. Li and L. Tang, *Electrochem. Commun.*, 11 (2009) 846
30. Y. Li, W. Gao, L. Ci, C. Wang and P.M. Ajayan, *Carbon*, 48 (2010) 1124
31. S. Sharma, A. Ganguly, P. Papakonstantinou, X.P. Miao, M.X. Li, J.L. Hutchison, M. Delichatsios and S. Ukleja, *J. Phys. Chem. C*, 114 (2010) 19459
32. Y. Xin, J. Liu, Y. Zhou, W. Liu, J. Gao, Y. Xie, Y. Yin and Z. Zou, *J. Power Sources*, 196 (2011) 1012
33. S.M. Choi, M.H. Seo, H.J. Kim and W.B. Kim, *Carbon*, 49 (2011) 904
34. S. Bong, Y.R. Kim, I. Kim, S. Woo, S. Uhm, J. Lee and H. Kim, *Electrochem. Commun.*, 12 (2010) 129
35. L.F. Dong, R.R.S. Gari, Z. Li, M.M. Craig and S.F. Hou, *Carbon*, 48 (2010) 781
36. C. Nethravathi, E.A. Anumol, M. Rajamathi and N. Ravishankar, *Nanoscale*, 3 (2011) 569
37. C. Xu, X. Wang and J.W. Zhu, *J. Phys. Chem. C*, 112 (2008) 19841
38. S. Yang, K. Chang, Y. Lee, C.M. Ma and C. Hu, *Electrochem. Commun.*, 12 (2010) 1206
39. R. Lv, T. Cui, M.S. Jun, Q. Zhang, A. Cao, D.S. Su, Z. Zhang, S.H. Yoon, J. Miyawaki, I. Mochida and F. Kang, *Adv. Funct. Mater.*, 21 (2011) 999
40. R.I. Jafri, T. Arockiados, N. Rajalakshmi and S. Ramaprabhu, *J. Electrochem. Soc.*, 157 (2010) B874
41. N. Jha, R.I. Jafri, N. Rajalakshmi and S. Ramaprabhu, *Int. J. Hydrogen Energy*, 36 (2011) 7284
42. P. Kundu, C. Nethravathi, P.A. Deshpande, M. Rajamathi, G. Madras and N. Ravishankar, *Chem. Mater.*, 23 (2011) 2772
43. W.S. Hummers and R.E. Offeman, *J. Am. Chem. Soc.*, 80 (1958) 1339
44. D.C. Marcano, D.V. Kosynkin, J.M. Berlin, A. Sinitskii, Z. Sun, A. Slesarev, L.B. Alemany, W. Lu and J.M. Tour, *Acs Nano*, 4 (2010) 4806
45. Y. Xu, K. Sheng, C. Li and G. Shi, *J. Mater. Chem.*, 21 (2011) 7376
46. H. Zhang, X. Xu, P. Gu, C. Li, P. Wu and C. Cai, *Electrochim. Acta*, 56 (2011) 7064
47. V. Radmilovic, H.A. Gasteiger and P.N. Ross, *J. Catal.*, 154 (1995) 98
48. C.L. Green and A. Kucernak, *J. Phys. Chem. B*, 106 (2002) 1036
49. D.K. Kang, C.S. Noh, N.H. Kim, S. Cho, J.M. Sohn, T.J. Kim and Y. Park, *J. Ind. Eng. Chem.*, 16 (2010) 385
50. H. Liu, C. Song, L. Zhang, J. Zhang, H. Wang and D.P. Wilkinson, *J. Power Sources*, 155 (2006) 95
51. I.M. Hsing, X. Wang and Y.J. Leng, *J. Electrochem. Soc.*, 149 (2002) A615
52. W. Sugimoto, K. Aoyama, T. Kawaguchi, Y. Murakami and Y. Takasu, *J. Electroanal. Chem.*, 576 (2005) 215
53. Z.B. Wang, G.P. Yin, Y.Y. Shao, B.Q. Yang, P.F. Shi and P.X. Feng, *J. Power Sources*, 165 (2007) 9

54. F. Ye, S. Chen, X. Dong and W. Lin, *J. Nat. Gas Chem.*, 16 (2007) 162
55. H. Yuan, D. Guo, X. Qiu, W. Zhu and L. Chen, *J. Power Sources*, 188 (2009) 8
56. M. Yen, M. Hsiao, S. Liao, P. Liu, H. Tsai, C.M. Ma, N. Pu and M. Ger, *Carbon*, 49 (2011) 3597
57. Q. Cheng, J. Tang, J. Ma, H. Zhang, N. Shinya and L. Qin, *Phys. Chem. Chem. Phys.*, 13 (2011) 17615
58. S. Yang, K. Chang, H. Tien, Y. Lee, S. Li, Y. Wang, J. Wang, C.M. Ma and C. Hu, *J. Mater. Chem.*, 21 (2011) 2374